



Full Text View

Volume 32, Issue 6 (June 2002)

Journal of Physical OceanographyArticle: pp. 1975–1986 | [Abstract](#) | [PDF \(440K\)](#)

Subduction along a Midocean Front and the Generation of Intrathermocline Eddies: A Theoretical Study^{*}

Hsien-Wang Ou and Arnold Gordon*Lamont-Doherty Earth Observatory, Columbia University, Palisades, New York*

(Manuscript received March 15, 2001, in final form November 19, 2001)

DOI: 10.1175/1520-0485(2002)032<1975:SAAMFA>2.0.CO;2

ABSTRACT

Through an idealized model, the authors consider the dynamics of subduction along a midocean front and its linkage to the intrathermocline eddies (ITEs). The subduction is necessitated by advective–diffusive balance of potential vorticity (PV), with its flux mainly a function of the mixed layer depth over the normal range of the horizontal diffusivity. The mismatch of PV impedes the entry of the subducted water into the interior, resulting in an excess flux that peaks at some intermediate mixed layer depth. This mismatch also causes the generation of anticyclonic ITEs, whose radius contains no lower bound, and a maximum limited by the entrainment rate. Through entrainment cooling, ITEs may leave their imprints in the surface temperature, giving rise to a meandering appearance of the front, even in the absence of instability.

1. Introduction

Midocean subpolar fronts separate warm and cold water masses and represent outcrops of the thermocline into the mixed layer. Hydrographic observations ([Pollard 1986](#)) show that the mixed layer water in the frontal zone is often subducted into the thermocline, contributing to ventilation of the latter. Moreover, recent observations ([Riser et al. 1986](#); [Eriksen et al. 1991](#); [Gordon et al. 2002](#)) suggest that the subducted water does not just ease into the interior, but sometimes manifests as isothermal blobs embedded in the thermocline, hence termed “intrathermocline eddies (ITE)” ([Dugan et al. 1982](#); [Kostianoy and Belkin 1989](#)). An example of ITE is shown in [Fig. 1](#) (reproduced from Fig. 3 of [Gordon et al. 2002](#)), which lies just south of the subpolar front in the Japan Sea. The section was taken in October 1999, but its water can be traced to the winter mixed layer in the frontal zone, suggesting its linkage to the subduction process.

Table of Contents:

- [Introduction](#)
- [Model configuration](#)
- [Subduction](#)
- [Intrathermocline eddy](#)
- [Summary and discussion](#)
- [REFERENCES](#)
- [APPENDIX](#)
- [FIGURES](#)

Options:

- [Create Reference](#)
- [Email this Article](#)
- [Add to MyArchive](#)
- [Search AMS Glossary](#)

Search CrossRef for:

- [Articles Citing This Article](#)

Search Google Scholar for:

- [Hsien-Wang Ou](#)
- [Arnold Gordon](#)

Can the subduction process be linked to the generation of intrathermocline eddies? What is their significance in modifying the water mass properties? It is the desire to address these questions—thus furthering our understanding of the phenomena—that motivates the present study.

As regards past studies, it should be noted that the subduction we are concerned with is a frontal phenomenon, thus quite distinct from that forced by the large-scale wind curl or surface cooling—a problem that is more widely explored in the literature (e.g., [Luyten et al. 1983](#); [Marshall and Nurser 1992](#)). For the frontal problem, most modeling studies involve a numerical integration of the primitive equations when an initial front is allowed to relax ([Wang 1993](#); [Spall 1995](#); [Yoshikawa et al. 2001](#)). Such fronts are observed to develop instability, and the accompanying transverse motion can force subduction—and upwelling—in the frontal zone. Of particular significance, [Spall \(1995\)](#) demonstrated that the subducted water might evolve into ITEs when the integration is carried out long enough, supporting a dynamical linkage of the two.

Since subpolar fronts are persistent, albeit time-varying, features, we present here a different view of the subduction process based on time-averaged balances. To elucidate the essential physics, we consider a highly simplified model that is amenable to analytical treatment. For the organization of the paper, we first describe the model configuration in [section 2](#). We then discuss the subduction process in [section 3](#), and its possible linkage to intrathermocline eddies in [section 4](#). The main findings of the model are summarized in [section 5](#), as well as additional discussion.

2. Model configuration

The model configuration is shown in [Fig. 2](#), which is intended to model a winter front when water masses are more sharply defined. As marked in the figure, the frontal zone represents a vertical extension of the thermocline into the mixed layer, where vertical mixing has rendered the density and flow fields vertically uniform. We neglect the alongfrontal variation and adopt a right-handed Cartesian coordinate system, with positive x and y directions referred respectively as eastward and poleward—as for the subpolar front in the Northern Hemisphere. For simplicity, both warm and cold water masses straddling the frontal zone are assumed homogeneous in density. For the former, one may invoke mixing by mesoscale eddies, which also homogenizes the potential vorticity (PV). For the cold water mass, its homogeneity can be attributed to surface cooling and convection—processes that produced the deep water. Since no geostrophic shear may be sustained without stratification, and given its great depth, the cold water mass is assumed motionless.

In our conceptualization, therefore, the frontal zone is not just a thermal feature, but also a transition region whereby the flow velocity from the warm side is reduced to zero. It should be stressed that, since the frontal zone is explicitly resolved, there can be no discontinuity in buoyancy or velocity at its cold edge. Since in the absence of alongfrontal variations, the mass continuity implies that the total cross-frontal transport is zero, whatever the influx of warm water into the frontal zone, it must be wholly subducted before the cold edge, and returns within the thermocline. This volume flux (at $y = 0$) is henceforth referred as the subduction flux—the primary property to be determined from the model. Since for the large-scale fronts of concern here the cause for the differing water masses is the differential surface heating, there must be a poleward buoyancy flux in the steady state, taken to be external to the model. Moreover, given the narrowness of the frontal zone (compared with the planetary scale), this flux is assumed a constant across the frontal zone—irrespective of local air–sea fluxes. As we shall see later, this poleward buoyancy flux, together with the total buoyancy difference across the frontal zone, define the scale of the subduction flux.


To examine the subsequent fate of the subducted water, we assume that internal mixing during the subduction process would render the subducted water vertically homogeneous, which may then be described as an intrathermocline “layer.” Properties of this layer before it is subjected to significant diabatic exchange with the ambient water define its upstream conditions. Such a three-layer configuration (warm, cold, and intrathermocline) represents a reasonable idealization of the observed situation, and is the simplest that allows one to address the evolution of the subducted water on its journey into the interior. Since the intrathermocline layer is sandwiched between a turbulent warm layer and a quiescent cold layer, its only diabatic exchange with the ambient water is assumed through an upward entrainment across its top surface. If the intrathermocline layer contains anticyclonic eddies (of extended center core), entrainment would be enhanced, thus affecting mass and property balances.

For simplicity, the model derivation will proceed in nondimensional forms. With b_* denoting the buoyancy of the warm layer (above that of the cold layer), H the unperturbed thermocline depth, f the Coriolis parameter (assumed constant in the frontal zone), and F_b the (constant) poleward buoyancy flux, the scaling rules (indicated by brackets) are defined as $[b] = b_*$, $[z] = H$, $[y] = R_C \equiv f^{-1}(b_*H)^{1/2}$ (the Rossby deformation radius), $[u] = fR_C$, $[v] = F_b(b_*H)^{-1}$, $[w] = [v]HR_C^{-1}$, $[\kappa]$ (horizontal diffusivity) $= [v]R_C$, $[q]$ (PV) $= fH^{-1}$, and wind and frictional stresses by $[\tau] = \rho_0 fH[v]$. In the following, we shall first consider the problem of subduction, and then its linkage to intrathermocline eddies.

3. Subduction

The aim here is to examine how the thermal and dynamical balances in the frontal zone, together with the far-field conditions, may constrain the subduction flux.

a. Heat balance

To formulate the heat balance in the frontal zone, we decompose the buoyancy flux into the advective flux associated with a mean cross-frontal circulation and the diffusive flux parameterized through a horizontal (eddy) diffusivity. As this diffusivity embodies turbulent motions in the mixed layer, its value is inherently uncertain. For simplicity, a constant value is nonetheless assigned, which will be varied over a wide range to underscore its uncertainty. As seen in [Fig. 2](#) , the advective flux (at any y) is facilitated by a poleward transport $V(y)$ of lighter water of buoyancy $b(y)$ in the mixed layer and a return of denser water underneath of equal transport (see [section 2](#)). If one neglects the horizontal diffusion below the mixed layer, the buoyancy flux carried by the return flow equals that exiting the base of the mixed layer poleward of y , so that

$$\text{advective buoyancy flux} = Vb - \int_0^y b \, dV$$

$$\text{for } 0 < y < l, \quad (3.1)$$

where l marks the width of the frontal zone. One doesn't know how V varies in the frontal zone except, like buoyancy, it decreases to zero at the poleward edge. For simplicity, we assume the two to be spatially similar so that

$$V/V_0 = b, \quad (3.2)$$

where the subscript 0 is used henceforth to denote the value at $y = 0$, with V_0 being the subduction flux to be determined. The need to adopt a specific form, such as [\(3.2\)](#), reflects the physics not considered in the model, which however does not impact on its main findings. With [\(3.2\)](#), it is trivial to see that the return flow carries a (transport-weighted) mean buoyancy half that of the overlying water so that [\(3.1\)](#) becomes

$$\text{advective buoyancy flux} = \frac{1}{2}Vb \quad \text{for } 0 < y < l. \quad (3.3)$$

Combining advective and diffusive fluxes, the heat balance thus states


$$\frac{1}{2}Vb - Kb_y = 1 \quad \text{for } 0 < y < l, \quad (3.4)$$

where the subscript y denotes a spatial derivative and

$$K = h_m \kappa \quad (3.5)$$

will be referred as the total diffusivity—being the product of the horizontal diffusivity κ and the mixed layer depth h_m . Since this depth is controlled mainly by vertical mixing independent of the frontal processes, it is assumed external to the model. Partly for this reason, there is no physical basis to adopt a particular distribution of the mixed layer depth across the (narrow) frontal zone, which thus is taken to be a constant for simplicity. Given the strong seasonal variation of this depth, however, it will be varied over the full range when the parameter dependence of the model solution is examined. One notes that because of the scaling, the poleward buoyancy flux on the rhs of [\(3.4\)](#) has a unit magnitude. It is clear from this equation that horizontal diffusion is required for resolving the frontal field and hence essential for the model. But with its inclusion, the heat balance no longer by itself implies a finite V —or subduction—since the buoyancy flux can be wholly accomplished by diffusion. As we shall see next, however, this is not the case for the vorticity balance, which demands a subduction in the presence of horizontal diffusion.

b. Vorticity balance

To formulate the vorticity balance in the frontal zone, let us first define the upper layer as consisting of the warm layer above the thermocline ($z > -h$ for $y < 0$) and the mixed layer within the frontal zone ($z > -h_m$ for $0 < y < l$), as shaded in [Fig. 2](#) . Since the flow contains no vertical shear in this layer ([section 2](#)), PV may be defined as a local property of the layer and governed by [from [\(A.8\)](#), in dimensional form]

$$\nabla \cdot [h(\mathbf{v}q - \kappa \nabla q)] = \mathbf{k} \cdot \nabla \times [h^{-1}(\boldsymbol{\tau} - \mathbf{F})]$$

for $y < l$, (3.6)

where $\boldsymbol{\tau}$ is the wind stress, and \mathbf{F} the frictional stress at the base of the layer. If one integrates this equation from the far field ($y \approx -\infty$) to the frontal zone, and nondimensionalizes the variables, one obtains an equation analogous to (3.4)

$$Vq - Kq_y = F_q \quad \text{for } 0 < y < l, \quad (3.7)$$

where

$$q = h_m^{-1}(1 - u_y) \quad (3.8)$$

$$F_q = [F_q]_{-\infty} - [h^{-1}\mathbf{i} \cdot (\boldsymbol{\tau} - \mathbf{F})]_{-\infty}^y \quad (3.9)$$

are respectively PV and PV flux in the frontal zone. As discussed in [appendix A](#), (3.6) holds irrespective of entrainment or subduction through the base of the layer, as encapsulated in the impermeability theorem of PV ([Haynes and McIntyre 1990](#)). In other words, the PV flux is more conservative than PV since a diabatic mass flux would alter the horizontal transport in inverse proportion to PV so that the PV flux remains unchanged.

Conceptually, one may set the far field at the equator where the PV flux ideally vanishes (due to hemispheric symmetry). Given also the shallowness of the mixed layer (compared with the thermocline in the far field), the sign of (3.9) is likely determined by the stresses in the frontal zone. Since the alongfrontal flow is seen later to be eastward, the frictional stress is positive, which would favor subduction. The wind stress, on the other hand, can be of either sign (or zero), and hence may or may not drive subduction [in fact, the subpolar front is typically situated under westerly—opposite of that required for subduction via (3.7)]. To underscore the fundamental nature of the subduction as inherent to the frontal phenomenon, we shall therefore concentrate on the case of zero PV flux and show that indeed the solution is characterized by subduction. The effect of a nonzero (but constant) PV flux—due to wind or frictional stress—will be discussed later ([section 3d](#)) in the context of how the basic solution is modified.

c. Solution

We now have [Eqs. \(3.2\), \(3.4\), \(3.7\), and \(3.8\)](#) governing the variables b , V , q , and u , which can be solved subjected to the boundary conditions discussed below (see [section 2](#)). Since buoyancy and PV are assumed homogenized in the warm layer, they are of unit magnitude by scaling definitions, or

$$b = q = 1 \quad \text{at } y = 0. \quad (3.10)$$

Assuming additionally that u in the warm layer satisfies the Margules equation, it is seen in [appendix B](#) to have the magnitude

$$u = 1 - h_m \quad \text{at } y = 0, \quad (3.11)$$

which is thus stronger when the mixed layer is shallower. At the cold edge of the front, we have on the other hand

$$b = u = 0 \quad \text{at } y = l, \quad (3.12)$$

where the frontal width l is as yet unknown. As seen in [appendix C](#), the model is hereby closed, and an analytical solution can be obtained given the external (dimensionless) parameters: the mixed layer depth h_m , the horizontal diffusivity κ , and the PV flux F_q . It is noted that no boundary condition is imposed on q at the cold edge. This is because PV may be defined as (3.8)—and hence governed by (3.7)—only where there is an upper layer; and, with PV undefined beyond the cold edge, no matching condition is required.

Before we present the solution, it is recalled that the model is more applicable to the winter front ([section 2](#)), and as representative of such a front, one may take a total temperature difference across the frontal zone to be 10 K so that the buoyancy of the warm layer is $b_* = 1 \text{ cm s}^{-2}$. Setting $H = 200 \text{ m}$ and $f = 10^{-4} \text{ s}^{-1}$, one estimates $R_C \approx 14 \text{ km}$, $[u] \approx 1.4 \times 10^2 \text{ cm s}^{-1}$, and $[q] \approx 5 \times 10^{-9} \text{ cm}^{-1} \text{ s}^{-1}$. Using a poleward heat flux of $1.3 \times 10^{11} \text{ W km}^{-1}$ (see, e.g., [Voorhis et al. 1976](#)), one estimates additionally $[v] \approx 1.5 \text{ cm s}^{-1}$, $[w] \approx 2.1 \times 10^{-2} \text{ cm s}^{-1}$, $[\tau] \approx 3 \text{ dyn cm}^{-2}$, and $[\kappa] \approx 2 \times 10^6 \text{ cm}^2 \text{ s}^{-1}$. A typical mixed layer depth is 100 m, which would yield $h_m = 0.5$. For the horizontal diffusivity, we follow [Taylor](#)

(1915) and use velocity and spatial scales of 10 cm s^{-1} and 10 km for eddies to yield a diffusivity of $10^7 \text{ cm}^2 \text{ s}^{-1}$, or in dimensionless units, $\kappa = 5$.

The solution using above dimensionless values and zero PV flux ($h_m = 0.5$, $\kappa = 5$, $F_q = 0$) is plotted in [Fig. 3](#). As expected, there is a poleward volume flux in the mixed layer V , which is depleted by subduction in the frontal zone. With the corresponding poleward decrease of the advective buoyancy flux, the diffusive flux must increase to accommodate the same total flux (3.4), causing a sharpening of the density gradient. As noted in (3.11), there is an eastward flow (and negative current shear) just outside the frontal zone. As this current decreases to zero at the cold edge, the negative shear gives way to positive shear, resulting in a velocity maximum in the frontal zone. The poleward increase of the cyclonic shear gives rise to an increase in PV—with the relative vorticity attaining a magnitude comparable to the Coriolis parameter. In other words, the dynamics in the frontal zone may not be quasigeostrophic, and one needs to be cautious in inferring the vertical velocity based on such assumption.

For an observational validation, [Pollard and Regier \(1992\)](#), for example, clearly shows the presence of a frontal jet, which moreover would support a poleward increase of PV. A direct comparison of the latter however cannot be made since most calculations of PV are carried out for density intervals, rather than for the upper layer. When converted to dimensional units, the solution shown in [Fig. 3](#) is quite sensible. The frontal jet has a peak speed of 1 m s^{-1} , the frontal width is 40 km , and the maximum poleward velocity is 3 cm s^{-1} .

Based on the above solution, we offer a simple explanation of the subduction as inherent to the frontal phenomenon: The shoaling of the thermocline to the mixed layer depth and the increase of the cyclonic vorticity as the frontal jet adjusts to zero cause a poleward increase of PV and, hence, a diffusive flux toward the warm side. In the absence of wind or frictional stress, this diffusive flux must be balanced by poleward advection of the lower PV water, which is then subducted via continuity. It is noted that with zero PV flux, the vorticity [equation \(3.7\)](#) is homogeneous, containing no forcing terms. Nor have we considered the mechanics that drives the ageostrophic cross-frontal flow. But to the extent that the solution is uniquely determined, the subduction may be regarded as forced by turbulence that gives rise to horizontal diffusion in the frontal zone and the large-scale processes that set up the far-field conditions.

While the above argument based on the vorticity balance offers a qualitative explanation of subduction, it gives no indication as to the magnitude of the subduction flux, which requires consideration of the buoyancy balance as well, as seen in the next section.

d. Parameter dependence

We plot in [Fig. 4](#) the subduction flux (solid lines) and the frontal width (dashed lines) as functions of the dimensionless parameters for the case of zero PV flux. The solid circle marks the solution shown in [Fig. 3](#). One notes first of all that as diffusivity or mixed layer depth (hence the total diffusivity) decreases, the frontal zone narrows. This dependence can be surmised from the heat balance (3.4) by noting that the diffusive flux is bounded above by unity, so a smaller total diffusivity would be accompanied by a sharper gradient and hence a narrower frontal zone. Quantitatively, it is seen that for a diffusivity of the order estimated earlier, the frontal zone spans a few Rossby deformation radii.

For the subduction flux, it is a weak function of the diffusivity, which can be explained as follows: At a given mixed layer depth, PV attains the same maximum at the cold edge if one neglects the relative vorticity for a moment and, since a larger diffusivity is associated with a wider front, the diffusive PV flux remains unchanged, and so is the subduction flux needed for the balance. If one now includes the relative vorticity, the maximum PV would be slightly smaller with larger diffusivity (since the front is wider), thus weakening the diffusive flux. This implies a smaller subduction flux, which can account for the slight tilt of the solid lines.

To explain the dependence of the subduction flux on the mixed layer depth, one notes first of all that a deeper mixed layer implies a weaker eastward jet outside the frontal zone (3.11). Reinforced by a wider frontal zone, the cyclonic vorticity at the cold edge, hence the PV there, is smaller. This would weaken the vorticity diffusion—hence the subduction flux—as the depth effects on the total diffusivity (3.5) and PV (3.8) otherwise cancel out. This variation of the subduction flux notwithstanding, it is of $O(1)$ over the medium range of the mixed layer depth—in support of its scaling by the poleward buoyancy flux.

To assess the effect of wind or frictional stress on the subduction, we have plotted in [Fig. 5](#) the solution corresponding to [Fig. 3](#), but with $F_q = -1$. As seen from (3.9), for a mixed layer depth of 0.5, this PV flux can be

achieved by a combination of zero PV flux in the far field, an eastward wind stress of 1.5 dyn cm^{-2} and zero frictional stress. Compared with [Fig. 3](#), it is seen that the subduction flux is reduced, the reason being that the diffusive flux in (3.7) is now partially balanced by the PV flux on the rhs, thus weakening the subduction. The weakened advection in turn implies via (3.4) a sharper density gradient and hence a narrower frontal zone. It is interesting to see that instead of

producing a frontal convergence, an eastward wind actually curtails the poleward flow in the frontal zone to weaken the subduction. It should be pointed out that the Ekman dynamics does not apply in the frontal zone, but is supplanted by the more general balance (3.7). Based on this solution, effects of other processes can be inferred: The frictional stress, for example, would generate a positive PV flux, thus enhancing the subduction and widening the frontal zone.

Given the noisy frontal environment, testing the above dependence from observation is obviously difficult. Although the frontal width can be monitored, say, by remote sensing of the surface temperature, its strong dependence on the highly uncertain diffusivity has lessened the significance of its prediction. The subduction flux, on the other hand, is more difficult to measure observationally, but its insensitivity to diffusivity and strong dependence on the mixed layer depth—which varies seasonally—may offer a better prospect for an observational assessment. One however is mindful of the seasonal variation of the poleward buoyancy flux that defines the scale of the subduction flux; the greater buoyancy flux in winter, for example, may (or may not) overcome the effect of a deepening mixed layer in weakening the subduction.

With above discussion, we have concluded our examination of the frontal balances and how they may constrain the subduction flux. We now proceed to examine the subsequent fate of the subducted water, and its possible linkage to the intrathermocline eddies.

4. Intrathermocline eddy

As alluded to in section 2, the departure point of the following discussion is the “upstream” intrathermocline layer, which has been rendered vertically homogeneous by internal mixing during subduction, but not yet modified by diabatic exchange with the ambient water.

a. Upstream condition

Since internal mixing does not change fluxes of buoyancy or PV, one may set their upstream values to the transport-weighted means of the subducted water exiting the base of the mixed layer (hence labeled by the subscript m). These mean properties are derived in appendix D, based on the frontal solution. For the buoyancy, it turns out that

$$b_m \equiv V_0^{-1} \int_0^{V_0} b \, dV = \frac{1}{2}, \quad (4.1)$$

or the mean buoyancy of the subducted water is simply half that of the warm layer.

The expression for the mean PV (D.2) is more complicated, containing both the subduction flux V_0 (via α of [C.2]) and the PV flux F_q . For the case of zero PV flux, it has however a simple expression

$$q_m \equiv V_0^{-1} \int_0^{V_0} q \, dV = \frac{1 - V_0/6}{1 - V_0/2}. \quad (4.2)$$

Since, as seen in Fig. 4, the subduction flux is insensitive to changing diffusivity, its value along the dotted line ($\kappa = 5$) is redrawn in Fig. 6 along with the mean PV (4.2). As expected from discussion in section 3d, the mean PV is greater for a shallower mixed layer, but unlike the subduction flux, which is bounded above by the buoyancy balance, the mean PV can in principle increase indefinitely as the mixed layer shallows.

With the specification of the upstream condition of the intrathermocline layer, one now proceeds to examine its downstream evolution.

b. Excess subduction flux

As we have discussed in section 2, the diabatic exchange between the intrathermocline layer and its ambient is through an entrainment across its upper surface. Since such entrainment does not change the density of the source water, the latter retains its upstream value. With the subscript i denoting the “interior” value (i.e., where the thermocline remains unperturbed), one has then

$$b_i = b_m = 1/2. \quad (4.3)$$

For the PV, on the other hand, it is conserved only if the entrainment is weak (relative to advection), which will be

assumed later to be the case. But as discussed above, a more general conservation principle, as entailed in the impermeability theorem, is that of the PV flux, which holds regardless the strength of the entrainment. For the present application, we follow the same steps as those leading to (3.7), but with the end points of integration being the upstream point of the intrathermocline layer and its downstream mergence with the unperturbed thermocline. Recalling that we have neglected the horizontal diffusion in the subsurface layer and neglecting also the frictional stresses acting on the layer, the vorticity balance then becomes

$$V_0 q_m = V_i \varepsilon^{-1}, \quad (4.4)$$

where V_i is the (unknown) volume flux into the interior thermocline and ε the thickness of the unperturbed thermocline—an external parameter. Rearranging the above equation, one has

$$V_i = \varepsilon q_m V_0; \quad (4.5)$$

the volume flux entering the interior thermocline thus may differ from that of the subducted water if there is a mismatch in PV. Let this difference be denoted by ΔV , one has then


$$\Delta V \equiv V_0 - V_i = V_0(1 - \varepsilon q_m). \quad (4.6)$$

It is seen in particular

$$\Delta V > 0 \quad \text{if } \varepsilon q_m < 1; \quad (4.7)$$

that is, if the interior thermocline is sufficiently thin, it would block out a portion of the subduction flux, an excess that must be disposed of by entrainment into the warm layer. It is important to distinguish therefore between the subduction flux that exits the base of the mixed layer and the flux that actually enters the interior thermocline and contributes to its ventilation—a distinction perhaps not sufficiently emphasized in the literature.

One also perceives the other possibility of $\varepsilon q_m > 1$ when (4.6) implies a transport deficit. How might this reconcile with the one-way entrainment? Since in this case, the interior thermocline poses no impediment to the entry of the subducted water, one may argue that the latter is simply embedded in the former, so there is no deficit in the transport. One may also argue that the excessive thickness of the thermocline, since not propped up by the incoming water, would simply be eroded away by local mixing. In any event, given the observed thinness of the thermocline (when compared with the winter mixed layer), such occurrences are likely infrequent.

Since both V_0 and q_m in (4.6) are mainly functions of the mixed layer depth (Fig. 6 ) , so is the excess flux ΔV , which is plotted in the same figure for $\varepsilon = 0.1$. As expected, except for very shallow mixed layer not likely realized in winter, ΔV is positive. Moreover, this excess flux peaks at some intermediate depth, the reason for which is as follows: As the mixed layer deepens, there is a greater mismatch of PV of the subducted water to that of the interior thermocline, which would dam out a greater *portion* of the subduction flux; but, since the subduction flux itself is smaller, the *absolute* excess flux thus exhibits a local maximum.

This excess flux can be disposed of by entrainment into the upper layer, and, since the entrainment rate is higher across a shallower interface, one expects a part of the excess flux to recirculate in the vicinity of the frontal zone where thermocline shoals. But if, for some reason, the subduction route is punctuated by anticyclonic eddies with their domed surfaces, the recirculation cell can extend farther into the interior. The generation of these eddies as an integral part of the subduction process is the subject to be examined next.

c. Eddy generation

As discussed in the introduction, ITEs have been observed near the front and they have been linked to the subduction process through water-mass properties. Dynamically, as explored extensively in the literature (Flierl 1979; Dugan et al. 1982; Spall 1995), conservation of PV as the subducted water seeks to merge with a thin thermocline induces a negative vorticity, and hence intrathermocline eddies of an extended center core. Common to the solutions cited above, the eddy radius is a free parameter, whose selection obviously requires other considerations. In Spall's (1995) initial-value problem, for example, eddies are the byproduct of baroclinic instability, and hence their size is scaled by the Rossby deformation radius.

Since the condition for the generation of anticyclonic eddies is precisely that for the existence of the excess subduction flux (4.7), we propose a different scenario for the generation of ITEs based on steady-state balances: as the mixed layer water is subducted, only a part of it may enter the interior thermocline because of the vorticity constraint. The rest would be dammed up in the form of anticyclonic eddies. These eddies would grow in size until the entrainment loss through their

domed surfaces equals the excess flux that feeds the eddies. This balance holds even if the eddy is moving along the front (by advection or self-propagation), which would set an upper bound on the eddy size. The reason why it is an upper bound is because eddies need not graze one another and, as mentioned earlier, some of the excess flux may recirculate without going through the eddies. For a crude scale derivation, let this maximum radius be denoted by R and the entrainment rate by w_e (all are nondimensionalized as before), the above mass balance states then

$$2R\Delta V \approx \iint_{\text{eddy}} w_e dA = \overline{w_e} \pi R^2, \quad (4.8)$$

in which the overbar indicates an areal average. Rearranging (4.8) yields

$$R = 2\pi^{-1}(\overline{w_e})^{-1}\Delta V. \quad (4.9)$$

The eddy radius thus is proportional to the excess flux ΔV divided by the mean entrainment rate across the top of the eddy.

Although the entrainment rate is highly uncertain, some qualitative points can nevertheless be made from (4.9). First of all, there is no lower bound on the eddy size since the excessive flux can be zero; the model thus can account for the submesoscale eddies discussed by [McWilliams \(1985\)](#). Second, other than its dependence on the mixed layer depth, the eddy size is limited above only by the entrainment rate. An ITE anchored in a deep thermocline thus can achieve great size, which may possibly explain the large eddy observed by [Bane et al. \(1989\)](#) in the Sargasso Sea. Third, although the mixed layer depth undergoes seasonal change, the observed eddies should bias toward the maximum size since the dissipative timescale is long compared with seasons. That is, while one may observe eddies of different sizes at various stages of growing and decaying, there is always the relic of the largest eddy allowed by the mixed layer depth.

For a quantitative assessment of (4.9), we invoke [Pollard and Regier \(1992\)](#), their Fig. 15a) to assign an entrainment rate of order $10^{-2} \text{ cm s}^{-1}$, which has a dimensionless value of 0.5 (see [section 3c](#)). Based on [Fig. 6](#), the maximum eddy radius thus is about twice the Rossby deformation radius or 30 km, which is not inconsistent with the observation shown in [Fig. 1](#). One, of course, recognizes that the entrainment rate may vary over orders of magnitude, so the above comparison does not validate the proposed balance (4.9), but merely supports its plausibility.

5. Summary and discussion

Although the model is highly idealized, some qualitative deductions seem robust, as summarized below:

- A poleward flow in the frontal zone—and hence subduction—is necessitated by a backward diffusion of PV toward the warm side as the frontal jet adjusts to zero value at its cold edge.
- The subduction flux is insensitive to the horizontal diffusivity, but mainly a function of the mixed layer depth, being smaller (in dimensionless units) when the mixed layer is deeper.
- Because of the mismatch in PV, only a portion of the subducted flux may enter the interior thermocline, with the excess flux peaking at some intermediate mixed layer depth.
- The above mismatch of PV also causes the generation of anticyclonic ITEs, which provide a pathway for dispensing the excess flux through enhanced entrainment across their domed surfaces.
- The mass balance may place a constraint on the eddy radius, which contains no lower bound, and a maximum limited by the entrainment rate.
- Given the seasonal change of the mixed layer depth and slow decay of the ITEs, the observed eddy radius should bias toward this maximum.

Through this study, we have presented a view of subduction as inherent to the frontal phenomenon, which is generally accompanied by ITEs based on time-mean balances. As such, the eddies may span a wide range in size, which nonetheless are predominantly anticyclonic—both in contrast to eddies generated by baroclinic instability. Also of interest, the deeper mixed layer, in fact, would reduce the subduction rate, which may still be greater in winter owing to the increased buoyancy flux across the frontal zone. The reason that subduction is more pronounced in winter is due paradoxically to its greater impediment to enter the interior, resulting in ITEs of more extended center core.

With entrainment—hence cooling of the surface water—enhanced over their domes, ITEs may leave imprints in the surface temperature, which seems to be the case in Japan Sea (Gordon et al. 2002, comparing their Figs. 2 and 6). It is suggested therefore that the observed meandering of the subpolar front simply reflects the presence of ITEs, and need not be indicative of frontal instability. As the movement of these eddies are likely impeded by topography, they may account for the semistationary appearance of the meanders.

Acknowledgments


The work is supported by the Office of Naval Research through Grant N00014-99-1-0092, as part of the Japan/East Sea initiative. We have benefited from discussion with many participants of the project. We thank Claudia Giulivi, Craig Lee, Amy Bower, Heather Hunt Furey, and Lynne Tally, who have contributed to the data shown in Fig. 1. We thank Y. K. Yoshikawa and an anonymous reviewer for helpful comments, which have resulted in a much improved paper.

REFERENCES

- Bane J. M., L. M. O'Keefe, and D. R. Watts, 1989: Mesoscale eddies and submesoscale, coherent vortices: Their existence near and interaction with the Gulf Stream. *Mesoscale/Synoptic Coherent Structures in Geophysical Turbulence*, J. Nihoul and B. Jamart, Eds., Elsevier, 501–518.
- Dugan J. P., R. P. Mied, P. C. Mignerey, and A. F. Schuetz, 1982: Compact, intrathermocline eddies in the Sargasso Sea. *J. Geophys. Res.*, **87**, 385–393. [Find this article online](#)
- Eriksen C. C., R. A. Weller, D. L. Rudnick, R. T. Pollard, and L. A. Regier, 1991: Ocean frontal variability in FASINEX. *J. Geophys. Res.*, **96**, 8569–8592. [Find this article online](#)
- Flierl G. R., 1979: A simple model for the structure of warm and cold core rings. *J. Geophys. Res.*, **84**, 781–785. [Find this article online](#)
- Gordon A. L., C. F. Giulivi, C. M. Lee, A. Bower, H. H. Furey, and L. Talley, 2002: Japan/East Sea intrathermocline eddies. *J. Phys. Oceanogr.*, **32**, 1960–1974. [Find this article online](#)
- Haynes P. H., and M. E. McIntyre, 1990: On the conservation and impermeability theorems for potential vorticity. *J. Atmos. Sci.*, **47**, 2021–2031. [Find this article online](#)
- Kostianoy A. G., and I. M. Belkin, 1989: A survey of observations on intrathermocline eddies in the World Ocean. *Mesoscale/Synoptic Coherent Structures in Geophysical Turbulence*, J. Nihoul and B. Jamart, Eds., Elsevier, 821–841.
- Luyten J. R., J. Pedlosky, and H. Stommel, 1983: The ventilated thermocline. *J. Phys. Oceanogr.*, **13**, 292–309. [Find this article online](#)
- Marshall J. C., and A. J. G. Nurser, 1992: Fluid dynamics of oceanic thermocline ventilation. *J. Phys. Oceanogr.*, **22**, 583–595. [Find this article online](#)
- McWilliams J. C., 1985: Submesoscale coherent vortices in the ocean. *Rev. Geophys.*, **23**, 165–182. [Find this article online](#)
- Pollard R. T., 1986: Frontal surveys with a towed profiling conductivity/temperature/depth measurement package (Sea-Soar). *Nature*, **323**, 433–435. [Find this article online](#)
- Pollard R. T., and L. A. Regier, 1992: Vorticity and vertical circulation at an ocean front. *J. Phys. Oceanogr.*, **22**, 609–625. [Find this article online](#)
- Riser S. C., W. B. Owens, H. T. Rossby, and C. C. Ebbesmeyer, 1986: The structure, dynamics, and origin of a small-scale lens of water in the western North Atlantic thermocline. *J. Phys. Oceanogr.*, **16**, 572–590. [Find this article online](#)
- Spall M. A., 1995: Frontogenesis, subduction, and cross-front exchange at upper ocean fronts. *J. Geophys. Res.*, **100**, 2543–2557. [Find this article online](#)
- Taylor G. I., 1915: Eddy motion in the atmosphere. *Philos. Trans. Roy. Soc. London*, **140A**, 1–26.
- Voorhis A. D., E. H. Schroeder, and A. Leetmaa, 1976: The influence of deep mesoscale eddies on sea surface temperature in the North Atlantic subtropical convergence. *J. Phys. Oceanogr.*, **6**, 953–961. [Find this article online](#)
- Wang D. P., 1993: Model of frontogenesis: Subduction and upwelling. *J. Mar. Res.*, **51**, 497–513. [Find this article online](#)
- Yoshikawa Y., K. Akitomo, and A. Toshiyuki, 2001: Formation process of intermediate water in baroclinic current under cooling. *J. Geophys. Res.*, **106**, 1033–1051. [Find this article online](#)

APPENDIX A

6. Vorticity Equation of the Upper Layer

We are concerned with the vorticity equation in the upper layer (shaded in [Fig. 2](#) ) , which consists of the warm layer above the thermocline and the mixed layer in the frontal zone. One assumes that vertical mixing has rendered the flow vertically uniform so that a potential vorticity q may be defined as

$$q \equiv h^{-1} (f + \zeta), \quad (\text{A.1})$$

where

$$\zeta \equiv \mathbf{k} \cdot \nabla \times \mathbf{v} \quad (\text{A.2})$$

is the relative vorticity. One begins with the momentum equation of the form

$$\frac{d\mathbf{v}}{dt} + f\mathbf{k} \times \mathbf{v} = -\rho_0^{-1}\nabla p + h^{-1}(\boldsymbol{\tau} - \mathbf{F}), \quad (\text{A.3})$$

where h is the layer depth, $\boldsymbol{\tau}$ the wind stress, and \mathbf{F} the frictional stress associated with the current shear at the base of the layer. If one takes the curl of this equation, its vertical component is

$$\frac{\partial \zeta}{\partial t} + \nabla \cdot (h\mathbf{v}q) = \mathbf{k} \cdot \nabla \times [h^{-1}(\boldsymbol{\tau} - \mathbf{F})]. \quad (\text{A.4})$$

The continuity equation for the layer is given by

$$\frac{\partial h}{\partial t} + \nabla \cdot (h\mathbf{v}) = w_e, \quad (\text{A.5})$$

where w_e is the diabatic vertical velocity across the base of the layer (positive for entrainment and negative for subduction). For the turbulent fields (denoted by primes) that are inviscid and adiabatic, [\(A.4\)](#) and [\(A.5\)](#) combine to yield the conservation of PV

$$\frac{dq'}{dt} = 0 \quad (\text{A.6})$$

so that the turbulent flux of PV may be parameterized in terms of diffusivity κ ([Young 1987](#))

$$\overline{\mathbf{v}'q'} = -\kappa\nabla\bar{q}, \quad (\text{A.7})$$

where overbars denote the time means. Now taking the time mean of [\(A.4\)](#), neglecting terms involving h' , and applying [\(A.7\)](#), one obtains the equation governing the mean PV (dropping overbars hereafter)

$$\nabla \cdot [h(\mathbf{v}q - \kappa\nabla q)] = \mathbf{k} \cdot \nabla \times [h^{-1}(\boldsymbol{\tau} - \mathbf{F})], \quad (\text{A.8})$$

which states that divergence of the PV flux (by mean and turbulent flows) is balanced by the torque exerted by wind and frictional stresses. It is important to note that this equation holds irrespective of the diabatic vertical velocity w_e . This is because such velocity would alter the volume transport in inverse proportion to PV so that the mean advective flux remains unchanged. This is the essence of the impermeability theorem of PV ([Haynes and McIntyre 1990](#)).

7. Solution in the Warm Layer

In the warm layer, PV is homogenized to unity by scaling definition so that

$$q = h^{-1}(1 - u_y) = 1. \quad (\text{B.1})$$

Given that the warm layer has unit buoyancy and that the alongfrontal velocity satisfies the Margules equation, one has

$$u = -h_y. \quad (\text{B.2})$$

The two [equations \(B.1\) and \(B.2\)](#) can be combined to yield an ordinary differential equation governing the thermocline depth

$$h_{yy} - h = -1. \quad (\text{B.3})$$

Subjected to the boundary conditions that

$$h \rightarrow 1 \quad \text{as } y \rightarrow -\infty \quad (\text{B.4})$$

$$h = h_m \quad \text{at } y = 0, \quad (\text{B.5})$$

the solution is

$$h = 1 - (1 - h_m) e^y. \quad (\text{B.6})$$

Substituting this solution into [\(B.2\)](#), one derives that

$$u_0 = 1 - h_m, \quad (\text{B.7})$$

which links the alongfrontal velocity at the warm edge of the frontal zone (hence the subscript 0) to the mixed layer depth.

APPENDIX C

8. Solution in the Frontal Zone

Substituting [\(3.2\)](#) into [\(3.4\)](#) and rearranging, one obtains

$$K (\alpha^2 b^2 - 1)^{-1} db = dy, \quad (\text{C.1})$$

in which we have defined

$$\alpha \equiv (V_0/2)^{1/2}, \quad (\text{C.2})$$

with the subduction flux V_0 yet to be determined. Integrating [\(C.1\)](#), one obtains

$$y = -K(2\alpha)^{-1} \ln \left[\left(\frac{1 + \alpha}{1 - \alpha} \right)^{-1} \left(\frac{1 + \alpha b}{1 - \alpha b} \right) \right], \quad (\text{C.3})$$

which can be inverted (graphically) to render $b(y)$. Substituting [\(3.2\)](#) into [\(3.7\)](#) and using [\(C.1\)](#), one obtains

$$(1 - \alpha^2 b^2) \frac{dq}{db} + 2\alpha^2 b q = F_q. \quad (\text{C.4})$$

Dividing this equation by $(1 - \alpha^2 b^2)^2$ leads to

$$\frac{d}{db}[(1 - \alpha^2 b^2)^{-1} q] = (1 - \alpha^2 b^2)^{-2} F_q, \quad (\text{C.5})$$

which can be integrated to yield

$$\begin{aligned} q = & (1 - \alpha^2 b^2) \\ & \times \left\langle \frac{1}{1 - \alpha^2} + \frac{F_q}{2\alpha} \left\{ \frac{\alpha b}{1 - \alpha^2 b^2} - \frac{\alpha}{1 - \alpha^2} \right. \right. \\ & \left. \left. + \frac{1}{2} \ln \left[\left(\frac{1 + \alpha}{1 - \alpha} \right)^{-1} \left(\frac{1 + \alpha b}{1 - \alpha b} \right) \right] \right\} \right\rangle. \end{aligned} \quad (\text{C.6})$$

Integrating (3.8), one has

$$u = u_0 + \int_0^y (1 - h_m q) dy. \quad (\text{C.7})$$

Substituting from (C.6) and performing the integration, one obtains

$$\begin{aligned} u = & u_0 + y \\ & - h_m K \left\langle \left\{ \frac{1}{1 - \alpha^2} - \frac{F_q}{2\alpha} \left[\frac{\alpha}{1 - \alpha^2} + \frac{1}{2} \ln \left(\frac{1 + \alpha}{1 - \alpha} \right) \right] \right\} \right. \\ & \times (1 - b) \\ & \left. - \frac{F_q}{4\alpha} \left[b \ln \left(\frac{1 + \alpha b}{1 - \alpha b} \right) - \ln \left(\frac{1 + \alpha}{1 - \alpha} \right) \right] \right\rangle. \end{aligned} \quad (\text{C.8})$$

To determine the subduction flux V_0 , we apply the boundary conditions (3.12) to (C.3) and (C.8) to yield two equations governing the frontal width l ,

$$l = \frac{K}{2\alpha} \ln \left(\frac{1 + \alpha}{1 - \alpha} \right), \quad \text{and} \quad (\text{C.9})$$

$$h_m = \left[1 + K \left(\frac{1 - F_q/2}{1 - \alpha^2} \right) \right]^{-1} (1 + l). \quad (\text{C.10})$$

Eliminating l from (C.9) and (C.10), one obtains an equation linking the subduction flux V_0 to the external parameters h_m , κ , and F_q . For practical calculations of the solution, we select particular values of V_0 and K , then calculate successively l [from (C.9)], h_m [from (C.10)], and κ [from (3.5)], which then allow the graphing of V_0 and l as functions of h_m and κ , as depicted in Fig. 3. Once V_0 is calculated, one may then calculate b , V , q , and u as functions of y from (C.3), (3.2), (C.6), and (C.8) successively.

APPENDIX D

9. Mean Properties of the Subducted Water

Let b_m be the (transport weighted) mean buoyancy of the subducted water, one derives


$$\begin{aligned} b_m &= V_0^{-1} \int_0^{V_0} b \, dV = \int_0^1 b \, db \quad [\text{using (3.2)}] \\ &= \frac{1}{2}, \end{aligned} \tag{D.1}$$

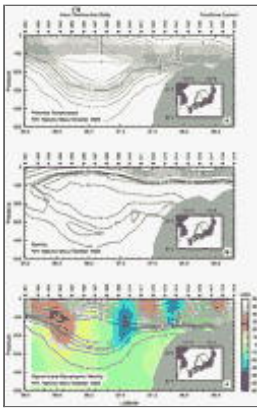
which sets the “upstream” buoyancy of the intrathermocline layer. Similarly, using (C.6), a straightforward integration yields

$$\begin{aligned} q_m &= V_0^{-1} \int_0^{V_0} q \, dV \\ &= \left[\frac{1 - F_q/2}{1 - \alpha^2} - \frac{F_q}{4\alpha} \ln\left(\frac{1 + \alpha}{1 - \alpha}\right) \right] \left(1 - \frac{V_0}{6}\right) \\ &\quad + \frac{F_q}{2V_0} \left\{ \left[1 + \alpha - \frac{1}{3}(1 + \alpha^3) \right] \ln(1 + \alpha) \right. \\ &\quad \quad \left. + \left[1 - \alpha - \frac{1}{3}(1 - \alpha^3) \right] \ln(1 - \alpha) \right. \\ &\quad \quad \left. - \frac{7}{9} + \frac{V_0}{3} \right\}, \end{aligned} \tag{D.2}$$

which links the “upstream” PV of the intrathermocline layer to the subduction flux and the PV flux in the frontal zone. It is noted, in particular, that

$$q_m = \frac{1 - V_0/6}{1 - V_0/2} \quad \text{if } F_q = 0, \tag{D.3}$$

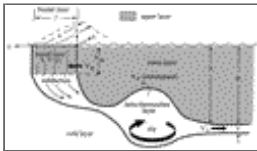
which is the value plotted in [Fig. 6](#) .



Click on thumbnail for full-sized image.

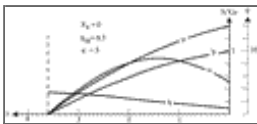
FIG. 1. Reproduced from Fig. 3 of [Gordon et al. \(2002\)](#) showing an ITE in the Japan Sea. The data are from the *Hakuho-Maru* section (the long section in the inset), obtained in Oct 1999. (a) The potential temperature, (b) salinity, and (c) σ_0 density.

Superimposed on the density section is the geostrophic velocity relative to 1000 db



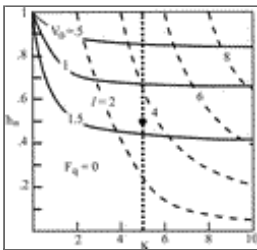
Click on thumbnail for full-sized image.

FIG. 2. The model configuration and symbols used in the model. The frontal zone represents an outcrop of the thermocline into the mixed layer. It is a transition region whereby buoyancy and flow of the warm layer decrease to zero at its cold edge. As such, the influx V_0 of warm water into the frontal zone is wholly subducted and returns within the thermocline. Because of mismatch of PV of the subducted water to that of the interior thermocline, part of the subduction flux is dammed up in the form of anticyclonic eddies, and expended by entrainment into the warm water





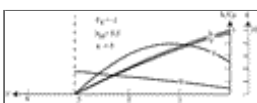
Click on thumbnail for full-sized image.

FIG. 3. Solutions in the frontal zone for the case of $F_q = 0$, $h_m = 0.5$, and $\kappa = 5$. As the eastward velocity u adjusts to zero at the cold edge, cyclonic vorticity is generated, which, together with shoaling of the thermocline, cause a poleward increase of the potential vorticity q . The resulting diffusive flux toward the warm side is balanced by the poleward flux V of the low PV warm water. As this flux is depleted by subduction, gradient of the buoyancy b is sharpened to accommodate the poleward buoyancy flux



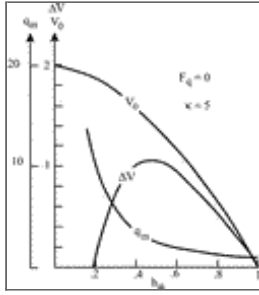
Click on thumbnail for full-sized image.

FIG. 4. Subduction flux V_0 and the frontal width l as functions of the mixed layer depth h_m and horizontal diffusivity κ , for the case of zero PV flux ($F_q = 0$). The frontal zone narrows for decreasing diffusivity or mixed layer depth, but the subduction flux is mainly a function of the mixed layer depth over the normal range of diffusivity. The solid circle marks the solution shown in [Fig. 3](#) . Properties along the dotted line are plotted in [Fig. 6](#) .



Click on thumbnail for full-sized image.

FIG. 5. Same as [Fig. 3](#) but for the case of $F_q = -1$. This PV flux can be achieved by a combination of zero PV flux in the far field, an eastward wind stress of 1.5 dyne cm^{-2} , and zero frictional stress (see [section 3c](#)). It is seen that the subduction flux and the frontal width have decreased from that shown in [Fig. 3](#).



[Click on thumbnail for full-sized image.](#)

FIG. 6. The subduction flux V_0 , the excess flux ΔV , and the mean PV of the subducted water q_m , plotted as functions of the mixed layer depth h_m for $F_q = 0$ and $\kappa = 5$ (i.e., along the dotted line in [Fig. 4](#)). It is seen that the excess flux has a maximum at some intermediate mixed layer depth due to the decreasing trends in both V_0 and q_m as h_m increases

* Lamont-Doherty Earth Observatory Contribution Number 6311.

Corresponding author address: Hsien-Wang Ou, Lamont-Doherty Earth Observatory of Columbia University, Rt. 9W, Palisades, NY 10964. E-mail: dou@ldeo.columbia.edu

[top](#) ▲



© 2008 American Meteorological Society [Privacy Policy and Disclaimer](#)
 Headquarters: 45 Beacon Street Boston, MA 02108-3693
 DC Office: 1120 G Street, NW, Suite 800 Washington DC, 20005-3826
amsinfo@ametsoc.org Phone: 617-227-2425 Fax: 617-742-8718
 Allen Press, Inc. assists in the online publication of AMS journals.